Title: Spatiotemporal expansion of primary progenitor zones in the developing human cerebellum

Authors: Parthiv Haldipur[1], Kimberly A. Aldinger[1], Silvia Bernardo[2], Mei Deng[3], Andrew E. Timms[4], Lynne M. Overman[5], Conrad Winter[6], Steven N. Lisgo[5], Ferechte Razavi[7], Evelina Silvestri[8], Lucia Manganaro[9], Homa Adle-Biasette[10], Fabien Guilmiot[11], Rosa Russo[12], Debora Kidron[13], Patrick R. Hof[14], Dianne Gerrelli[15] Susan J. Lindsay[4], William B. Dobyns[1,3], Ian A. Glass[1,3], Paula Alexandre[15], Kathleen J. Millen [1,3]*

Affiliations:

[1]Center for Integrative Brain Research, Seattle Children's Research Institute, Seattle, WA, 98101, USA.

[2]Department of Experimental Medicine, Sapienza University of Rome, 00185 Rome, Italy.

[3]Department of Pediatrics, University of Washington, Seattle, WA, 98195, USA.

[4]Center for Developmental Biology and Regenerative Medicine, Seattle Children's Research Institute, Seattle, WA 98101, USA

[5]Institute of Genetic Medicine, Newcastle University, International Centre for Life, Central Parkway, Newcastle upon Tyne NE1 3BZ, UK

[6]Department of Pathology, Seattle Children's Hospital, Seattle, WA 98105, USA

[7]Unité d'Embryofœtopathologie, Service d'Histologie-Embryologie-Cytogénétique, Hôpital Necker-Enfants Malades, APHP, 75015 Paris, France

[8]Surgical Pathology Unit, San Camillo Forlanini Hospital, 00152 Rome, Italy.

[9]Department of Radiological Sciences, Sapienza University of Rome, 00185 Rome, Italy.
[10]Department of Pathology, Hôpital Lariboisière, APHP, 75010 Paris, UMR1141, Université Paris   Diderot, Sorbonne Paris Cité, France

[11]Hôpital Robert-Debré, INSERM UMR 1141, 75019 Paris, France.

[12]Department of Pathology, Molecular Genetics Laboratory, University Medical Hospital, 84131 Salerno, Italy

[13]Pathology Department, Meir Medical Center, Kfar Saba, 4428164, Israel.

[14]Nash Family Department of Neuroscience and Friedman Brain Institute, Icahn School of Medicine at Mount Sinai, New York, NY 10029, USA

[15]Developmental Biology and Cancer Unit, Great Ormond Street Institute of Child Health, University College London, London WC1N 1EH, UK.

*Correspondence to: Kathleen J. Millen: kathleen.millen@seattlechildrens.org

One Sentence Summary
Unique human cerebellar progenitor populations limit validity of mouse-centric models of human neurodevelopmental disorders

Abstract
We present the first histological and molecular analysis of the developing human cerebellum from 30 post-conception days to 9 postnatal months. Significant differences in developmental patterns between human and the well characterized mouse model include spatiotemporal expansion of both ventricular and rhombic lip primary progenitor zones to include sub-ventricular zones containing outer radial glia with cerebellar specific molecular signatures. The long-lived human rhombic lip undergoes multiple morphological changes culminating in the formation of an internalized progenitor pool in the posterior lobule, with no equivalent in any model organism, including the macaque. Disruptions in human rhombic lip development are associated with posterior cerebellar vermis hypoplasia and Dandy-Walker malformation. Species differences in progenitor populations challenge current mouse-centric paradigms of human cerebellar disease mechanisms.

The human cerebellum contains 80% of all neurons of the human brain (Lange, 1975). Birth defects of the cerebellum are common, poorly understood, and cause diverse developmental outcomes as well as significant motor and cognitive disabilities, including autism (Aldinger and Doherty, 2016). Despite the overwhelming number of neurons it contains, and the clinical importance of cerebellar birth defects, very little is known about the developmental and molecular biology of the human cerebellum. In fact, most evidence is inferred from studies carried out in animal models, especially the mouse (Leto et al., 2016). As the salient features that define the cerebellum, such as lamination, circuitry, neuronal morphology and foliation are largely conserved in the mouse and human, it has long been assumed that cerebellar developmental mechanisms are also conserved (Larsell, 1970; Larsell, 1972), in spite of notable differences between these species. For example, the total surface area of the human cerebellum is 750-fold greater than in the mouse (Van Essen, 2002). The mouse cerebellum accounts for only 60% of all its brain neurons (Lange, 1975). The human cerebellum exhibits disproportionate expansion of cerebellar hemispheres and significantly increased folial complexity relative to the mouse. Additionally, neuronal scaling differs between the two species: in the mouse, the granule cell to Purkinje cell (PC) ratio is 200:1 whereas in humans, this ratio is 3000:1 (Lange, 1975).

Human cerebellar development initiates during the first post-conception month and is not complete until the end of the second postnatal year (Rakic and Sidman, 1970; Haldipur et al., 2011; Biran et al., 2012; Haldipur et al., 2012). This is in stark contrast to the mouse in which cerebellar development is complete by postnatal day 15, following only 19 days of gestation. Protracted development in humans alone is unlikely to explain all species differences. Recent studies have uncovered substantial differences in cerebral cortical neurogenesis between mice and humans during development. Human cerebral cortical expansion and foliation is driven by elaboration of the subventricular zone (SVZ) and the emergence of large numbers of outer radial glia (oRG) in an outer subventricular zone (oSVZ) that is absent in mice (Lui et al., 2014; Molnar and Pollen, 2014; Nowakowski et al., 2016). As cerebellar neuron numbers scale with cerebral cortical neuron numbers across evolution (Herculano-Houzel, 2010), we hypothesized that cerebellar neurogenesis programs are also divergent across these species.

Studies of human cerebellar development are rare. Initial studies were conducted prior to publication of photographic plates (Larsell, 1947; Larsell and Stotler, 1947). Although limited histological data is available from 10 post-conception weeks (pcw) through late gestation (Rakic and Sidman, 1970; Zecevic and Rakic, 1976; Abraham et al., 2001; Haldipur et al., 2011; Haldipur et al., 2012), there is little accompanying molecular data. Neuroimaging atlases have been compiled from extensive *in utero* MRI studies. These provide valuable volumetric and growth parameters useful for some aspects of clinical prenatal diagnoses, yet only cover gestational weeks (gw) 20-24 (18-22 pcw) , and important histological features are not resolvable (Habas et al., 2010a; Habas et al., 2010b). Major gaps in available human data correspond to essential cerebellar developmental epochs that have been defined in model vertebrates (Leto et al., 2016). To address these specific limitations, we present the first ever comprehensive analysis of human cerebellar development from post-conception day 30 to 9 postnatal months, (**Fig. 1**) comprising 80 samples **(Table S1).** We define the timing of crucial developmental events and provide the first insights into both evolutionarily conserved and divergent cellular and molecular programs driving human cerebellar development. Not only are

our data relevant to basic science, they fundamentally challenge the current mouse-centric models of pathogenesis of human cerebellar neurodevelopmental disorders.

Spatial expansion and temporal persistence of primary progenitor zones in the developing human cerebellum

To survey the morphology of human cerebellar development, we assessed Hematoxylin & Eosin stained sagittal vermis sections **(Fig. 1)**. As expected from mice, we identified two primary zones of neurogenesis: the ventricular zone (VZ) **(Fig. 1 and Fig. S1A, red arrowhead)**, and the rhombic lip (RL) **(Fig. 1 and Fig. S1A, black arrowhead)**. Mouse fate mapping experiments have demonstrated that the VZ gives rise to all GABAergic populations (PCs, a subset of deep cerebellar neurons, and interneurons) in overlapping waves of neurogenesis. The RL gives rise to all glutamatergic neurons in the cerebellum, beginning with deep cerebellar neurons, followed by granule cell precursors (GCPs) of the external granule layer (EGL) which divide extensively, then differentiate and migrate to become granule neurons of the internal granule layer (IGL), and unipolar brush cells (UBCs) (Leto et al., 2016). Between Carnegie Stage (CS) 12 to CS23 (30- 56 days), the developing human cerebellar anlage resembled the size and relative shape of the mouse cerebellar anlage from embryonic day (E) 10.5-17.5 (**Fig. 1 and Fig. S1A**). Yet even at these early stages there were notable differences. The mouse VZ rapidly thins between E10.5 and E15.5 **(Fig. S1B-G, VZ)** and the RL disappears by birth **(Fig. S1A, black arrowhead)**. The human embryonic RL was small and similar to the mouse, yet the human VZ rapidly thickened through 10 pcw, with a concurrent bulging of the cerebellar anlage. After 10 pcw, the human cerebellar VZ thinned, while the previously small RL dramatically expanded into an elongated tail-like structure not previously described in any vertebrate. Between 11-13 pcw, the elongated human RL thickened, yet continued to trail from the growing posterior vermis. Strikingly, between 13-14 pcw, this stem cell zone became incorporated within the posterior lobule where it formed a densely packed pool of cells with a residual population present as late as 36 pcw.

The mouse EGL is evident by e12.5, with GCP proliferation (peaking at post-natal day [P] 6) driving postnatal cerebellar and foliation expansion (Dahmane and Ruiz i Altaba, 1999; Corrales et al., 2004; Blaess et al., 2008). We detected initial EGL formation in the human cerebellum by 8 pcw with primary and secondary fissure initiation apparent at 11 pcw and 13 pcw respectively. Between 17 pcw and birth (~36 pcw) there was a dramatic (~5 fold) increase in human cerebellar volume and folial complexity (Chang et al., 2000; Limperopoulos et al., 2005; Volpe, 2009). Peak proliferation of granule cell precursors in the human EGL is known to occur between 26-32 pcw (Abraham et al., 2001).

The developing human cerebellar ventricular zone has a subventricular zone with outer radial glia

The bulging of the early human cerebellar VZ prompted further analysis. CS12 was the only stage at which the human cerebellar VZ resembled that of the mouse, which displays a single zone of SOX2$^+$, KI67$^+$ progenitor cells spanning most of the anlage at E12.5 **(Compare Fig. 2A with Figure S1B, F)**. By CS14, just three days later, an emerging human SVZ was also evident **(Fig. 2B)**. By CS18 and CS19, a cell sparse inner SVZ and cell dense outer SVZ were clear **(Fig. 2C, D)**, with differentiating nascent (TUJ1$^+$, CTIP1$^+$) neurons expanding into the

anlage increasing cerebellar anlage size and contributing to anlage bulging **(Fig. 2H, I)**. Increased differentiation in the outer SVZ diminished SVZ size between CS21 and CS23 **(Fig. 2E, F)**. By the end of the Carnegie Stages of embryogenesis, at 8 pcw, only a residual VZ remained **(Fig. 2G)**.

The presence of progenitor cells in a human cerebellar SVZ is striking and reminiscent of the developing mouse and human cerebral cortex (Pollen et al., 2015). The mouse cerebellar VZ does not have a SVZ. Mouse cerebellar ventricular radial glial progenitors extend processes across the entire anlage from the ventricular (apical) surface to the pial (basal) surface and undergo mitosis only at the ventricle **(Fig. S1L-Q)**. However, in the human embryonic cerebellum, we observed PH3$^+$ progenitors in mitosis within the VZ and SVZ **(Fig. 2J, K)**. Progenitors in both zones exhibited long radial processes and expressed the mitotic radial glial marker phospho-vimentin, with evidence of an interrupted scaffold of fibers between the VZ and SVZ similar to the extensive oRG progenitors in the human cerebral cortex **(Fig. 2J-M)**. We conclude that the human cerebellar VZ, unlike the mouse, undergoes considerable expansion and structural changes across embryogenesis. Our data confirm that the VZ of the developing human cerebellum is expanded into an SVZ with oRG cells. This represents the first demonstration that oRG are present outside of the developing human cerebral cortex.

The human cerebellar rhombic lip is long-lived, undergoes complex morphogenesis and also has a SVZ with oRG

Species differences in progenitor zone development were not restricted to the cerebellar VZ. We also identified dramatic species differences in RL morphology, finding elaborate RL sub-structure in humans including splitting into ventricular (RL^{VZ}) and subventricular zones (RL^{SVZ}), and occupying an "internalized" position, correlating with growth and foliation of the human posterior vermis **(Fig. 3 A-G)**. The mouse RL is a highly proliferative, transient, dorsal stem cell zone, present between E12.5 and E17.5, and composed entirely of KI67 and SOX2$^+$ stem cells lacking apparent morphological compartmentalization **(Fig. S2A-E)**. Although the mouse RL is between 5 and 8 cell layers thick, mitosis of progenitors identified by phospho-histone H3 and phospho-Vimentin staining is confined to the one layer of cells lining the ventricle. by **(Fig. S2G-L)**. In contrast, the human RL and its remnants were seen throughout gestation **(Fig. 3 A-G)** and displayed a more complex proliferation profile.

The unexpected morphology of the human RL led us to confirm that it excluded VZ derived GABAergic neurons and was highly proliferative. This was particularly important at stages later than 13 pcw, when the RL became embedded within the posterior-most lobule of the cerebellum **(Figs. 3H-K; 4A)**. In the embryonic cerebellum (CS12-23), the simple RL, much like in the mouse, consisted of cells expressing KI67 and SOX2 **(Compare Fig. 4A, B; CS18 with Fig. S2 A-F, RL, red asterisk)**. However, after 10 pcw the RL split into a SOX2- and KI67-rich ventricular zone (RL^{VZ}) **(Fig. 4A, B; red asterisk)** and a KI67-rich, SOX2-sparse subventricular zone (RL^{SVZ}) **(Fig. 4A, B; yellow asterisk)**. The two RL progenitor zones were separated by an extensive vasculature bed, readily discernable by 11 pcw, yet still present even at later stages **(Fig. S3A, B)**. Cells in the RL^{SVZ} were apparently streaming into the EGL **(Fig. 4A, 8, 10 and 17 pcw; red arrowhead)**

The similarities between the simple human embryonic and mouse RL extends to the location of radial glia in mitosis. Much like in the mouse RL, radial glial mitosis in the simple

human embryonic RL was confined to cells lining the ventricle **(Fig. 4C, D; CS18)**. However, following the split of the RL, mitotic radial glia (PH3^{+}, phospho-vimentin[+]) were detected in both the RL^{VZ} **(Fig. 4C, 14 pcw; red asterisk)** and RL^{SVZ} **(Fig. 4C, 14 pcw; yellow asterisk)**. To identify the morphology of progenitors residing in the RL^{VZ} and RL^{SVZ}, we labeled acute slices of 21 pcw cerebellum with fine crystals of DiI (Saito et al., 2003). Following fixation, imaging, and 3D reconstruction, cells with radial glial morphology were apparent in both RL zones **(Fig. 4E)**.

Although the mouse RL lacks evident structural compartmentalization, it is molecularly compartmentalized by differential expression of several key genes. An interior Wntless (WLS[+]) and LMX1A^{+} compartment is continuous with the RL^{VZ} and an exterior compartment linked to the external granule layer (ATOH1^{+}). A gradient of PAX6^{+} expression exists across the mouse RL with strongest expression in the exterior compartment. The core of the mouse RL is composed of proliferating LMX1A^{+} progenitors destined to become posterior vermis EGL, GCPs and Unipolar brush cells (UBCs). Early specified and differentiating UBCs also in the core express TBR2 (Chizhikov et al., 2010; Yeung et al., 2014).

In human samples, similar to the mouse, at all stages, WLS expression was largely restricted to RL^{VZ} cells, although scattered expression was seen in RL^{SVZ} cells **(Fig. S4A-D).** *LMX1A* was expressed throughout the entire human RL at embryonic stages **(Fig. S4E)** and in both the RL^{VZ} and RL^{SVZ} at later stages **(Fig. S4F-H)**. *LMX1A* was also expressed in expected RL-derived cerebellar nuclear and UBC populations streaming into the cerebellar core as well as the choroid plexus epithelium **(Fig. S4E-H; CPe)**. We observed a sharp RL boundary between *LMX1A* and *ATOH1* in RL exiting cells at all stages delimiting the anterior limit of the RL **(compare Fig. S4E-H with J-M)**. GCPs and UBCs leaving the RL also expressed *ATOH1*, as expected from mouse **(Fig. S4J-M)**. The posterior limit of the human RL was defined by *LMX1A*^{+}, *MKI67*^{-} choroid plexus cells, as in mice **(Fig. S4E, I, J, dashed-line)**. In humans, strong PAX6 expression was predominant in the RL^{VZ}, although there was also extensive expression in the RL^{SVZ}, with upregulation in nascent EGL cells streaming from the RL **(Fig. S4N-Q)**. We found extensive TBR2 expression throughout the human RL^{SVZ} with a few scattered, presumably nascent UBCs in the EGL and IGL **(Fig. S4R-U)**.

Human RL progenitor programs demonstrate considerable divergence from human cerebral cortical progenitor molecular programs.

To provide an unbiased analysis of the molecular programs encoded by human RL progenitors we profiled the developing human RL transcriptome **(Data S1-S5)**. We used laser-capture microdissection (LCM) to isolate RL^{VZ} and RL^{SVZ} from sagittal sections of cerebellum (9 to 22 pcw). We isolated total RNA from 18 LCM-isolated samples (9 RL^{VZ} and 9 RL^{SVZ}) and performed bulk RNA-sequencing **(Data S1)**. After quality control and normalization, principal component analysis (PCA) indicated age as the first principal component explaining 56% of the variance **(Fig. 5A)**. Differential expression analysis between RL^{VZ} and RL^{SVZ} identified alterations in 462 genes (log$_2$ fold change > 1.5 and Benjamini-Hochberg adjusted *P* < 0.05). The 374 genes upregulated in RL^{VZ} included *CRYAB*, *SOX2*, *SOX9* and *WLS*, while the 88 genes upregulated in the RL^{SVZ} included *EOMES* **(Fig. 5B, C; Data S2)**. We evaluated pathway enrichment of the gene sets and found that RL^{VZ} genes were enriched in genes involving cell adhesion, anatomical structure morphogenesis, and negative regulation of gene expression and involved in WNT and HIPPO signaling. No pathway enrichment was found among the and RL^{SVZ}

gene set **(Data S3-S4)**. We next compared our human RL expression profiles to published profiles of radial glial populations in the human neocortex (Nowakowski et al., 2017) using gene set enrichment analysis (GSEA) (Subramanian et al., 2005). GSEA showed that each of these gene sets was significantly enriched in the RL^{VZ} **(Fig. 5C-E, Data S5)**. We conclude that although there are significant similarities across progenitors from different CNS regions, there are clearly many differences that most certainly reflect unique developmental programs for each region. The novel plan of cerebellar development is consistent with studies on human stem cell derived cerebellar neurons, which differ from mouse counterparts in aspects of their program (Sundberg et al., 2018).

The spatiotemporal expansion of the rhombic lip may be a human-specific feature

To determine the evolutionary origins of the spatiotemporal expansion profile of the RL and we sought to examine the developing cerebellum of a non-human primate. In the developing cerebral cortex, human and non-human primates share an expanded SVZ relative to mice, although differences exist in progenitor numbers, cell cycle dynamics, size and cortical gyrification (Lui et al., 2011; Borrell and Reillo, 2012; Florio and Huttner, 2014). Given that the ratio of brain weight by neuron number does not differ significantly among all primate brains (Azevedo et al., 2009; Herculano-Houzel, 2009; Lui et al., 2011), we expected non-human primates to share elaborated cerebellar progenitor zones. We obtained developing cerebellar tissue of rhesus macaque (*Macaca mulatta*; 164 days gestation) from the MacBrain Resource (macbrainresource.org). Mid-sagittal cerebellar vermis sections were available from 5 macaque fetuses spanning E48 to E87. Analysis of these sections demonstrated that the early macaque RL at E48 resembles the simple embryonic CS23 RL in humans **(Fig. 6A)**. However, as the first signs of foliation appear, the macaque RL regresses in a manner similar to the developing mouse cerebellum **(Fig. 6B, C)** and by mid-gestation (E78-87), we found no evidence of the expansion or morphological compartmentation seen during human RL development **(Fig. 6D-G)**. Although additional cerebellar samples from other primate species are unavailable; our developmental analysis of the macaque cerebellum is consistent with the conclusion that spatiotemporal expansion of the RL is specific to the developing human cerebellum.

One possible explanation for the spatiotemporal expansion of the human RL is that it may be a necessary feature of protracted gestation. We tested this hypothesis by examining archival sections from a single 8.5 gestational month (GM) male bottlenose dolphin (*Tursiops truncatus*; 12 months gestation) cerebellum. Although these animals are precocial and have an extensively foliated cerebellum, the posterior region from this sample was conspicuously lacking an internalized RL **(Fig. 6H)**. We are actively working to identify additional specimens from this species and other mammals with prolonged gestation. However, this preliminary analysis suggests that elaborated RL development does not directly correlate with gestational length.

The long-lived human 'internalized' rhombic lip is required to generate the posterior vermis

The volume of the developing human cerebellum increases 5 fold between 22 pcw and birth, and it becomes highly foliated during the third trimester (24-40 gw) (Chang et al., 2000; Limperopoulos et al., 2005; Volpe, 2009). This is also a period during which EGL proliferation peaks, accompanied by an increase in EGL thickness (Rakic and Sidman, 1970; Abraham et

al., 2001). In mice, extensive cerebellar growth and foliation is similarly driven EGL proliferation between post-natal days 1 and 14, with deficient proliferation resulting in thinning of EGL and subsequent reduction in cerebellar volume and reduced foliation complexity (Dahmane and Ruiz i Altaba, 1999). Reduced cerebellar volume is a primary feature of a many human cerebellar birth defects, particularly posterior fossa malformations including Dandy-Walker malformation (DWM) and cerebellar vermis hypoplasia (CVH) (Patel and Barkovich, 2002; Aldinger et al., 2009; Barkovich et al., 2009). Both of these structural birth defects display disproportionate posterior vermis hypoplasia (Russo and Fallet-Bianco, 2007; Kapur et al., 2009; Haldipur et al., 2017) **(Fig. 6I-N, arrowhead; Figure S5)**. Mouse models have indicated that RL disruption is central to posterior vermis hypoplasia (Chizhikov et al., 2010; Haldipur et al., 2014; Haldipur et al., 2017). In mice and humans, ten cardinal lobules are grouped together into anterior, central and posterior lobes of the vermis defined by the primary and secondary fissure. In humans, all ten lobules were first identifiable between 14 and 18 pcw. There was an anterior to posterior developmental gradient with posterior vermis size and folial complexity differentially increasing until at least 36 pcw **(Figure 1)**. Although there is no way to ascertain what the 'normal' RL looks like after 21 pcw due to the paucity of normal cerebellar tissue after 21 pcw, it is clear that the RL and its vestiges are still detectable in mid and late gestation cerebella until birth **(Fig. 1 and Fig. S3C)**, as seen in specimens from stillborn fetuses likely exposed to cardiovascular and pulmonary insults. The longevity of the internalized RL therefore correlates with growth and foliation of the human posterior vermis.

To determine if RL abnormalities contribute to human cerebellar malformations, we assessed 16 archival DWM and CVH cerebellar samples between 17 and 30 pcw **(Table S1, Figure S5A-P).** In these samples, we observed at least a delay, if not failure of posterior vermis growth as indicated by reduced posterior foliation and aberrant morphology. A common feature among the majority of cases was the presence of a partially formed posterior lobule (Haldipur et al., 2017). While it is possible that decreased EGL proliferation may contribute to this phenotype, peak EGL proliferation only begins around pcw 26 (26-32 pcw) (Abraham et al., 2001). Yet hypoplasia of the posterior vermis was clearly evident at these much earlier stages (Russo and Fallet-Bianco, 2007; Kapur et al., 2009; Bernardo et al., 2015; Haldipur et al., 2017) **(Fig. 6 I-N; Figure S5)**. Furthermore, these phenotypes are routinely diagnosed *in utero* around 17 pcw, suggesting an earlier origin of these defects (Poretti et al., 2016). In 50% of our cases, the RL was completely absent, while in the remaining samples, RL development was delayed (not internalized) and significantly reduced in size, lacking the normal dense hypercellularity **(Fig. 6M, N)**. Among cerebella lacking any RL, ~62% were older than 21 pcw **(Fig. 6; Table S1)**, when the human RL is normally still present. We therefore conclude that while the early simple RL contributes GCPs to the EGL which subsequently proliferate to drive expansion of the anterior cerebellum, the later, internalized human RL (post 14 pcw) is required to generate GCPs to fully elaborate the posterior vermis during mid and late gestation.

Preterm brain injury has been associated with cerebellar abnormalities (Limperopoulos et al., 2010; Pichiecchio et al., 2016; al, 2019). Notably, here we report that the cerebellar RL^{VZ} and RL^{SVZ} are separated by a vascular bed beginning at 11 pcw, when the RL itself is elongated and potentially quite vulnerable to vascular insult. Our morphological analysis of DWM and CVH cases suggests that vascular insults in the human RL from 13-14 pcw onwards could be major contributors to the developmental pathogenesis of these clinically important

neurodevelopmental abnormalities. Thus, although mouse studies were essential to spotlight a role for the RL in human cerebellar malformations like DWM (Aldinger et al., 2009; Haldipur et al., 2014; Haldipur et al., 2017), it is now clear that the underlying pathological mechanisms can never be fully modeled in mice, because mice lack critically important transient developmental zones seen in humans. Similarly, our discovery of previously undescribed progenitor populations and the longevity of the RL in the developing human cerebellum suggests that mouse models of the cells of origin for some groups of medulloblastoma may also be inadequate (Azzarelli et al., 2018).

In summary, this study provides the first comprehensive analysis of human cerebellar development, identifying critical features including spatial and temporal subventricular expansion of both the classical cerebellar VZ and the RL germinal zones. Notably, the generation of cerebellar neurons in these zones occurs over a different time scale under the control of apparently distinct gene expression programs compared to the well-studied mouse cerebellum. Our identification of significant numbers of oRG in both the human cerebellar VZ and RL demonstrates that this progenitor program is not exclusive to the developing human neocortex. The expansion of both human cerebellar SVZ zones is not concurrent with SVZ and oRG expansion in the developing human cerebral cortex which occurs in the second trimester (Saito et al., 2011). While human RL progenitors share some molecular features with human neocortical progenitors, there are distinct cerebellar signatures. We are not yet able to directly compare embryonic macaque cerebellar VZ development with early human embryonic cerebellar VZ development. However, macaques clearly do not exhibit RL expansion, suggesting that a multilayered substructure of the RL is unique to humans. Unlike the expansion of human oRG progenitors of the cortical SVZ, neither the cerebellar VZ/SVZ nor RL^{SVZ} oRG actively drive cerebellar foliation. We have instead provided evidence that the temporal persistence of the human RL is likely essential to expand and elaborate the human posterior cerebellar vermis. Our studies underline the urgency of further comparative cellular and molecular analyses of human and mouse cerebellar development to define better the value and limitations of mouse genetic models of human neurodevelopmental disorders.

Figure legends

Fig. 1: An outline of human cerebellar development. H&E-stained midsagittal sections through the human embryonic (CS12-CS23) and (8-36 pcw) cerebellar vermis. The two main zones of neurogenesis, the ventricular zone (red arrowhead) and rhombic lip (black arrow head) are marked. Primary and secondary fissures are noted (arrows). The human and mouse embryonic cerebellum are similar in shape and form between CS12 and CS23. The first sign of foliation appears around 11 pcw. There is a significant increase in size and foliation between 17 pcw and birth (36 pcw). Scale bar = 100 μm

Fig. 2: The human cerebellar ventricular zone is vastly expanded and contains a subventricular zone. Midsagittal sections of the human embryonic and cerebellum stained with KI67 (A-G) and SOX2 (D), indicating the expansion of the ventricular zone (VZ). β-III Tubulin (TUJ1) and CTIP1 expression indicate that neuronal differentiation takes place in the sub-ventricular zone (SVZ) and begins around CS19 (H, I). Mitosis is observed in both the VZ and SVZ (J) as indicated by phospho-histone H3 (PH3) expression. Mitotic radial glia marked by

phospho-vimentin (P-VIM) expression are present in both the VZ and SVZ (K-M) indicating the existence of ventricular and outer radial glia in the human embryonic cerebellum. All sections were counterstained using DAPI. mes indicates head mesenchyme on top of the pial surface (dotted line, red dash). Green and black dashed lines indicate the boundaries of the VZ and SVZ respectively. Scale bar = 100 μm (A-L, white) and 25 μm (M, red)

Fig. 3: Spatio-temporal expansion of the human cerebellar rhombic lip. The human cerebellar RL undergoes morphological transformations during development and provides granule cell precursors to the external granule layer. The human RL structurally resembles the mouse RL at CS19 (A). Between 8 and 12 pcw, it is elongated into a 'tail-like' structure (B, box). After 13 pcw the RL internalizes to form a pool of cells confined to the posterior-most lobule (C-G, box). The RL is not seen after birth (H). Purkinje cells (PCs) born in the ventricular zone (VZ), as indicated by CTIP1 (H, K) and CALB1 [Calbindin] (I, J) expression can be seen migrating around the RL region. Scale bar = 100 μm (A, black; H-K, white,), 500 μm (B-E, red), and 1 mm (F, G, green)

Fig. 4: The human cerebellar rhombic lip is compartmentalized into ventricular and subventricular zones. The human cerebellar RL is highly proliferative as indicated by KI67 expression (A). The RL is expanded into a SOX2-rich ventricular (red asterisk) and SOX2-sparse (yellow asterisk) subventricular zones (B). phosphohistone-H3 (C) and phospho-vimentin (D) expression indicate the presence of ventricular (red asterisk) and outer radial glia (yellow asterisk) in a state of mitosis. DiI labeling of an organotypic slice of a 21 pcw human cerebellum (E) reveals morphology of ventricular and outer radial glia in the RL. Scale bar = 100 μm (white), 50 μm (yellow), 20 μm (red), and 1 μm (blue).

Fig. 5: RNA-seq of human RL compartments. (A) Principal component (PC) analysis indicated that the largest source of variation among the RNA-seq samples was age accounting for 56% of the variance in the data. Samples microdissected from RL^{SVZ} are blue and RL^{VZ} are red. The numbers beside each circle represent age of the sample in pcw. (B) Volcano plot illustrating differential expression of genes in RL^{VZ} versus RL^{SVZ}. Red and blue dots represent genes expressed significantly higher in RL^{VZ} or RL^{SVZ}, respectively. (C-E) Comparison of the human RL expression profile to human cortical radial glia. Volcano plot illustrating differential expression of genes in RL^{VZ} versus RL^{SVZ}. Black dots represent genes with significant differential expression between RL^{VZ} and RL^{SVZ}. Purple dots represent genes from each gene set. GSEA showed that human cortical radial glia genes are all enriched in the RL^{VZ}.

Fig. 6: Internalized rhombic lip is a feature specific to human cerebellar development. Cresyl violet-stained sagittal sections of the macaque cerebellum at (A) E48, (B) E59, (C) E64, (D, E) E78, (F, G) E87, and (H) H&E-stained sagittal section of the cerebellum from a bottlenose dolphin of age 8.5 gestational months (GM) suggests that the rhombic lip is not a feature of all primates or animals with a prolonged gestation period, but rather a human-specific trait. Analysis of H&E-stained sagittal sections of the human cerebellum from cases diagnosed with DWM and CVH (I-N) indicates RL is absent in 50% of cases while in the remaining cases it was severely diminished (O). The anterior (a), central (c) and posterior lobes (p) are indicated. (O)

Pie chart representing the absence of rhombic lip in 50% of tested samples. Scale bar = 100 µm
(A-C, E, G, J, L, black), 0.5 mm (D, N, blue) and 1 mm (F, H, I, K, M, red)

References

Abraham, H., Tornoczky, T., Kosztolanyi, G. and Seress, L. (2001) 'Cell formation in the cortical layers of the developing human cerebellum', *International journal of developmental neuroscience : the official journal of the International Society for Developmental Neuroscience* 19(1): 53-62.

al, K. A. A. e. (2019) 'Redefining the etiologic landscape of cerebellar malformations', *Submitted to NEJM.*

Aldinger, K. A. and Doherty, D. (2016) 'The genetics of cerebellar malformations', *Seminars in fetal & neonatal medicine* 21(5): 321-32.

Aldinger, K. A., Lehmann, O. J., Hudgins, L., Chizhikov, V. V., Bassuk, A. G., Ades, L. C., Krantz, I. D., Dobyns, W. B. and Millen, K. J. (2009) 'FOXC1 is required for normal cerebellar development and is a major contributor to chromosome 6p25.3 Dandy-Walker malformation', *Nature genetics* 41(9): 1037-42.

Azevedo, F. A., Carvalho, L. R., Grinberg, L. T., Farfel, J. M., Ferretti, R. E., Leite, R. E., Jacob Filho, W., Lent, R. and Herculano-Houzel, S. (2009) 'Equal numbers of neuronal and nonneuronal cells make the human brain an isometrically scaled-up primate brain', *The Journal of comparative neurology* 513(5): 532-41.

Azzarelli, R., Simons, B. D. and Philpott, A. (2018) 'The developmental origin of brain tumours: a cellular and molecular framework', *Development* 145(10).

Barkovich, A. J., Millen, K. J. and Dobyns, W. B. (2009) 'A developmental and genetic classification for midbrain-hindbrain malformations', *Brain : a journal of neurology* 132(Pt 12): 3199-230.

Bernardo, S., Vinci, V., Saldari, M., Servadei, F., Silvestri, E., Giancotti, A., Aliberti, C., Porpora, M. G., Triulzi, F., Rizzo, G. et al. (2015) 'Dandy-Walker Malformation: is the 'tail sign' the key sign?', *Prenatal diagnosis* 35(13): 1358-64.

Biran, V., Verney, C. and Ferriero, D. M. (2012) 'Perinatal cerebellar injury in human and animal models', *Neurology research international* 2012: 858929.

Blaess, S., Stephen, D. and Joyner, A. L. (2008) 'Gli3 coordinates three-dimensional patterning and growth of the tectum and cerebellum by integrating Shh and Fgf8 signaling', *Development* 135(12): 2093-103.

Borrell, V. and Reillo, I. (2012) 'Emerging roles of neural stem cells in cerebral cortex development and evolution', *Developmental neurobiology* 72(7): 955-71.

Chang, C. H., Chang, F. M., Yu, C. H., Ko, H. C. and Chen, H. Y. (2000) 'Assessment of fetal cerebellar volume using three-dimensional ultrasound', *Ultrasound in medicine & biology* 26(6): 981-8.

Chizhikov, V. V., Lindgren, A. G., Mishima, Y., Roberts, R. W., Aldinger, K. A., Miesegaes, G. R., Currle, D. S., Monuki, E. S. and Millen, K. J. (2010) 'Lmx1a regulates fates and location of cells originating from the cerebellar rhombic lip and telencephalic cortical hem', *Proceedings of the National Academy of Sciences of the United States of America* 107(23): 10725-30.

Corrales, J. D., Rocco, G. L., Blaess, S., Guo, Q. and Joyner, A. L. (2004) 'Spatial pattern of sonic hedgehog signaling through Gli genes during cerebellum development', *Development* 131(22): 5581-90.

Dahmane, N. and Ruiz i Altaba, A. (1999) 'Sonic hedgehog regulates the growth and patterning of the cerebellum', *Development* 126(14): 3089-100.

Florio, M. and Huttner, W. B. (2014) 'Neural progenitors, neurogenesis and the evolution of the neocortex', *Development* 141(11): 2182-94.

Habas, P. A., Kim, K., Corbett-Detig, J. M., Rousseau, F., Glenn, O. A., Barkovich, A. J. and Studholme, C. (2010a) 'A spatiotemporal atlas of MR intensity, tissue probability and shape of the fetal brain with application to segmentation', *Neuroimage* 53(2): 460-70.

Habas, P. A., Kim, K., Rousseau, F., Glenn, O. A., Barkovich, A. J. and Studholme, C. (2010b) 'Atlas-based segmentation of developing tissues in the human brain with quantitative validation in young fetuses', *Human brain mapping* 31(9): 1348-58.

Haldipur, P., Bharti, U., Alberti, C., Sarkar, C., Gulati, G., Iyengar, S., Gressens, P. and Mani, S. (2011) 'Preterm delivery disrupts the developmental program of the cerebellum', *PLoS One* 6(8): e23449.

Haldipur, P., Bharti, U., Govindan, S., Sarkar, C., Iyengar, S., Gressens, P. and Mani, S. (2012) 'Expression of Sonic hedgehog during cell proliferation in the human cerebellum', *Stem cells and development* 21(7): 1059-68.

Haldipur, P., Dang, D., Aldinger, K. A., Janson, O. K., Guimiot, F., Adle-Biasette, H., Dobyns, W. B., Siebert, J. R., Russo, R. and Millen, K. J. (2017) 'Phenotypic outcomes in Mouse and Human Foxc1 dependent Dandy-Walker cerebellar malformation suggest shared mechanisms', *eLIFE* 6.

Haldipur, P., Gillies, G. S., Janson, O. K., Chizhikov, V. V., Mithal, D. S., Miller, R. J. and Millen, K. J. (2014) 'Foxc1 dependent mesenchymal signalling drives embryonic cerebellar growth', *eLife* 3.

Herculano-Houzel, S. (2009) 'The human brain in numbers: a linearly scaled-up primate brain', *Frontiers in human neuroscience* 3: 31.

Herculano-Houzel, S. (2010) 'Coordinated scaling of cortical and cerebellar numbers of neurons', *Frontiers in neuroanatomy* 4: 12.

Kapur, R. P., Mahony, B. S., Finch, L. and Siebert, J. R. (2009) 'Normal and abnormal anatomy of the cerebellar vermis in midgestational human fetuses', *Birth defects research. Part A, Clinical and molecular teratology* 85(8): 700-9.

Lange, W. (1975) 'Cell number and cell density in the cerebellar cortex of man and some other mammals', *Cell and tissue research* 157(1): 115-24.

Larsell, O. (1947) 'The development of the cerebellum in man in relation to its comparative anatomy', *The Journal of comparative neurology* 87(2): 85-129.

Larsell, O. and Stotler, W. A. (1947) 'Some morphological features of the human cerebellum', *The Anatomical record* 97(3): 352.

Larsell, O. a. J. J. (1970) 'The Comparitive Anatomy and Histology of Cerebellum from Monotremes through Apes', *University of Minnesota Press. Minneapolis*.

Larsell, O. a. J. J. (1972) 'The Comparative Anatomy and Histology of the Cerebellum. The Human Cerebellum, Cerebellar Connections and Cerebellar Cortex', *University of Minnesota Press. Minneapolis*.

Leto, K., Arancillo, M., Becker, E. B., Buffo, A., Chiang, C., Ding, B., Dobyns, W. B., Dusart, I., Haldipur, P., Hatten, M. E. et al. (2016) 'Consensus Paper: Cerebellar Development', *Cerebellum* 15(6): 789-828.

Limperopoulos, C., Folkerth, R., Barnewolt, C. E., Connolly, S. and Du Plessis, A. J. (2010) 'Posthemorrhagic cerebellar disruption mimicking Dandy-Walker malformation: fetal imaging and neuropathology findings', *Seminars in pediatric neurology* 17(1): 75-81.

Limperopoulos, C., Soul, J. S., Gauvreau, K., Huppi, P. S., Warfield, S. K., Bassan, H., Robertson, R. L., Volpe, J. J. and du Plessis, A. J. (2005) 'Late gestation cerebellar growth is rapid and impeded by premature birth', *Pediatrics* 115(3): 688-95.

Lui, J. H., Hansen, D. V. and Kriegstein, A. R. (2011) 'Development and evolution of the human neocortex', *Cell* 146(1): 18-36.

Lui, J. H., Nowakowski, T. J., Pollen, A. A., Javaherian, A., Kriegstein, A. R. and Oldham, M. C. (2014) 'Radial glia require PDGFD-PDGFRbeta signalling in human but not mouse neocortex', *Nature* 515(7526): 264-8.

Molnar, Z. and Pollen, A. (2014) 'How unique is the human neocortex?', *Development* 141(1): 11-6.

Nowakowski, T. J., Bhaduri, A., Pollen, A. A., Alvarado, B., Mostajo-Radji, M. A., Di Lullo, E., Haeussler, M., Sandoval-Espinosa, C., Liu, S. J., Velmeshev, D. et al. (2017) 'Spatiotemporal gene expression trajectories reveal developmental hierarchies of the human cortex', *Science* 358(6368): 1318-1323.

Nowakowski, T. J., Pollen, A. A., Sandoval-Espinosa, C. and Kriegstein, A. R. (2016) 'Transformation of the Radial Glia Scaffold Demarcates Two Stages of Human Cerebral Cortex Development', *Neuron* 91(6): 1219-1227.

Patel, S. and Barkovich, A. J. (2002) 'Analysis and classification of cerebellar malformations', *AJNR. American journal of neuroradiology* 23(7): 1074-87.

Pichiecchio, A., Decio, A., Di Perri, C., Parazzini, C., Rossi, A. and Signorini, S. (2016) '"Acquired" Dandy-Walker malformation and cerebellar hemorrhage: Usefulness of serial MRI', *European journal of paediatric neurology : EJPN : official journal of the European Paediatric Neurology Society* 20(1): 188-91.

Pollen, A. A., Nowakowski, T. J., Chen, J., Retallack, H., Sandoval-Espinosa, C., Nicholas, C. R., Shuga, J., Liu, S. J., Oldham, M. C., Diaz, A. et al. (2015) 'Molecular identity of human outer radial glia during cortical development', *Cell* 163(1): 55-67.

Poretti, A., Boltshauser, E. and Huisman, T. (2016) 'Pre- and Postnatal Neuroimaging of Congenital Cerebellar Abnormalities', *Cerebellum* 15(1): 5-9.

Rakic, P. and Sidman, R. L. (1970) 'Histogenesis of cortical layers in human cerebellum, particularly the lamina dissecans', *The Journal of comparative neurology* 139(4): 473-500.

Russo, R. and Fallet-Bianco, C. (2007) 'Isolated posterior cerebellar vermal defect: a morphological study of midsagittal cerebellar vermis in 4 fetuses--early stage of Dandy-Walker continuum or new vermal dysgenesis?', *Journal of child neurology* 22(4): 492-500; discussion 501.

Saito, K., Kawaguchi, A., Kashiwagi, S., Yasugi, S., Ogawa, M. and Miyata, T. (2003) 'Morphological asymmetry in dividing retinal progenitor cells', *Development, growth & differentiation* 45(3): 219-29.

Saito, T., Hanai, S., Takashima, S., Nakagawa, E., Okazaki, S., Inoue, T., Miyata, R., Hoshino, K., Akashi, T., Sasaki, M. et al. (2011) 'Neocortical layer formation of human developing brains and lissencephalies: consideration of layer-specific marker expression', *Cerebral cortex* 21(3): 588-96.

Subramanian, A., Tamayo, P., Mootha, V. K., Mukherjee, S., Ebert, B. L., Gillette, M. A., Paulovich, A., Pomeroy, S. L., Golub, T. R., Lander, E. S. et al. (2005) 'Gene set enrichment analysis: a knowledge-based approach for interpreting genome-wide expression profiles', *Proceedings of the National Academy of Sciences of the United States of America* 102(43): 15545-50.

Sundberg, M., Tochitsky, I., Buchholz, D. E., Winden, K., Kujala, V., Kapur, K., Cataltepe, D., Turner, D., Han, M. J., Woolf, C. J. et al. (2018) 'Purkinje cells derived from TSC patients display hypoexcitability and synaptic deficits associated with reduced FMRP levels and reversed by rapamycin', *Molecular psychiatry* 23(11): 2167-2183.

Van Essen, D. C. (2002) 'Surface-based atlases of cerebellar cortex in the human, macaque, and mouse', *Annals of the New York Academy of Sciences* 978: 468-79.

Volpe, J. J. (2009) 'Cerebellum of the premature infant: rapidly developing, vulnerable, clinically important', *Journal of child neurology* 24(9): 1085-104.

Yeung, J., Ha, T. J., Swanson, D. J., Choi, K., Tong, Y. and Goldowitz, D. (2014) 'Wls provides a new compartmental view of the rhombic lip in mouse cerebellar development', *The Journal of neuroscience : the official journal of the Society for Neuroscience* 34(37): 12527-37.

Zecevic, N. and Rakic, P. (1976) 'Differentiation of Purkinje cells and their relationship to other components of developing cerebellar cortex in man', *The Journal of comparative neurology* 167(1): 27-47.

was covered by a material transfer agreement between SCRI and HDBR/BDRL, but samples may be requested directly from the HDBR/BDRL. Images of the developing macaque cerebellum were provided by MacBrainResource: macbrainresource.org (NIMH R01-MH113257 to Drs. Alvaro Duque and Lynn Selemon). Sequence data have been deposited into dbGAP.
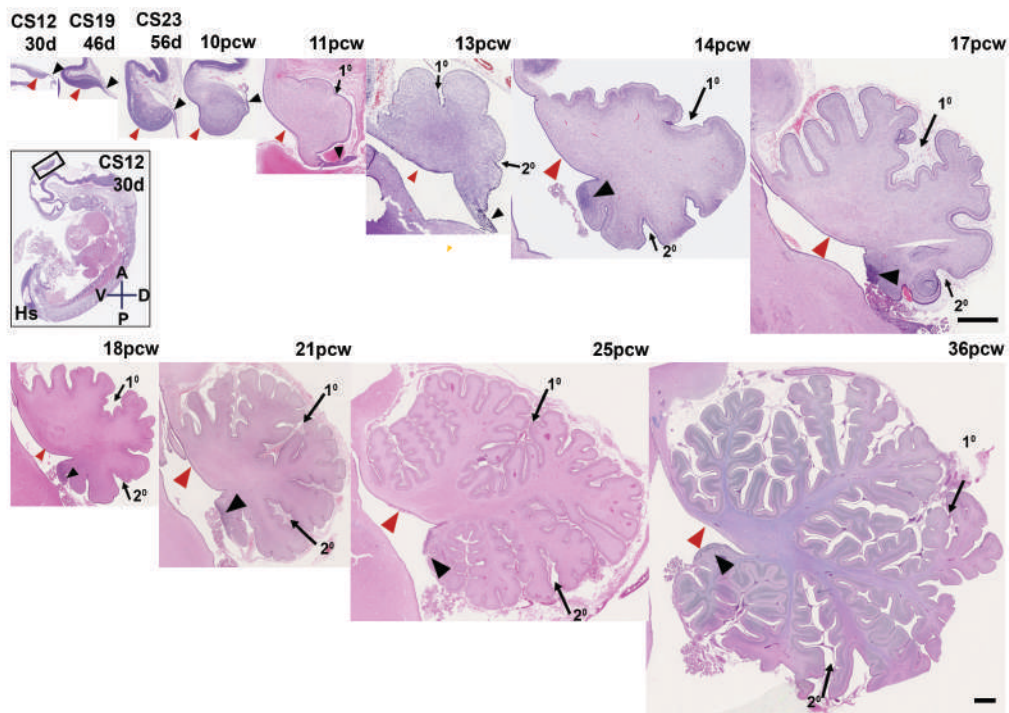
5

10

15

20

25

Figure 1

Fig. 1: An outline of human cerebellar development. H&E-stained midsagittal sections through the human cerebellar vermis. The two main zones of neurogenesis, the ventricular zone (red arrowhead) and rhombic lip (black arrow head) are marked. Primary and secondary fissures are noted (arrows). The human and mouse embryonic cerebellum are similar in shape and form between CS12 and CS23. The first sign of foliation appears around 11 pcw. There is a significant increase in size and foliation between 17 pcw and birth (36 pcw). Scale bar = 100 μm
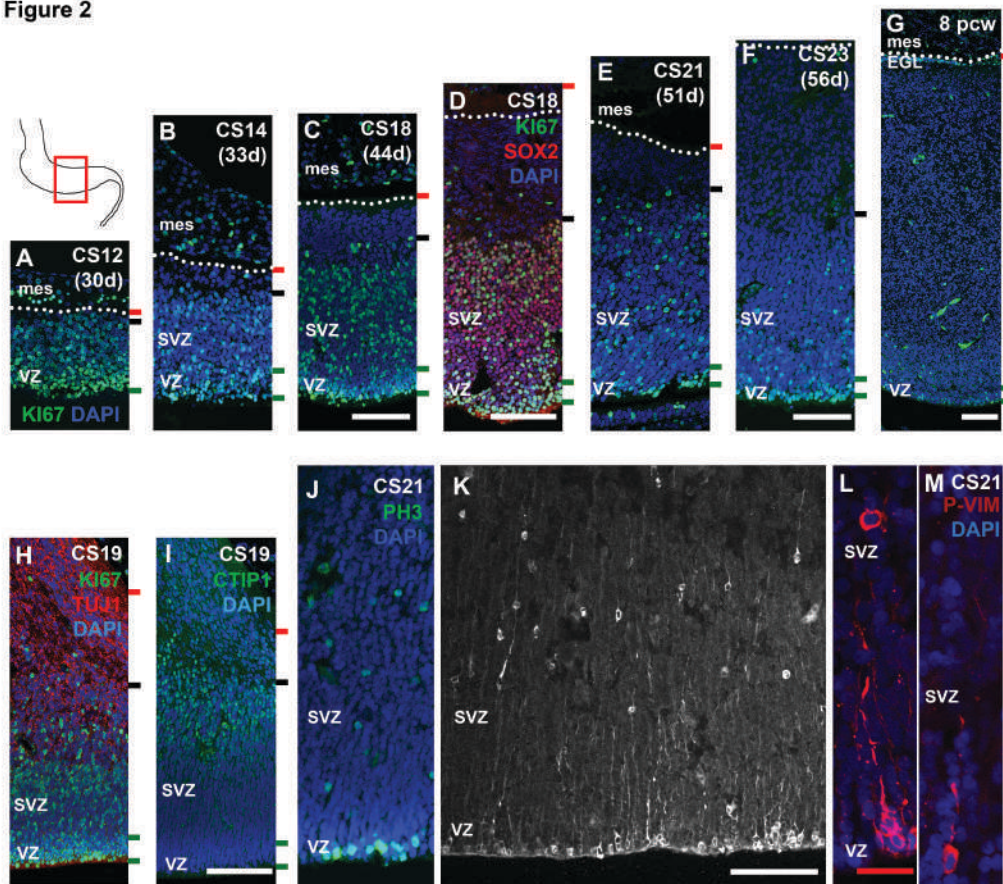
Fig. 2: The human cerebellar ventricular zone is vastly expanded and contains a subventricular zone. Midsagittal sections of the developing human cerebellum stained with KI67 (A-G) and SOX2 (D), indicating the expansion of the ventricular zone (VZ). β-III Tubulin (TUJ1) and CTIP1 expression indicate that neuronal differentiation takes place in the sub-ventricular zone (SVZ) and begins around CS19 (H, I). Mitosis is observed in both the VZ and SVZ (J) as indicated by phospho-histone H3 (PH3) expression. Mitotic radial glia marked by phospho-vimentin (P-VIM) expression are present in both the VZ and SVZ (K-M) indicating the existence of ventricular and outer radial glia in the human embryonic cerebellum. All sections were counterstained using DAPI. mes indicates head mesenchyme on top of the pial surface (dotted line, red dash). Green and black dashed lines indicate the boundaries of the VZ and SVZ respectively. Scale bar = 100 μm (A-L, white) and 25 μm (M, red)
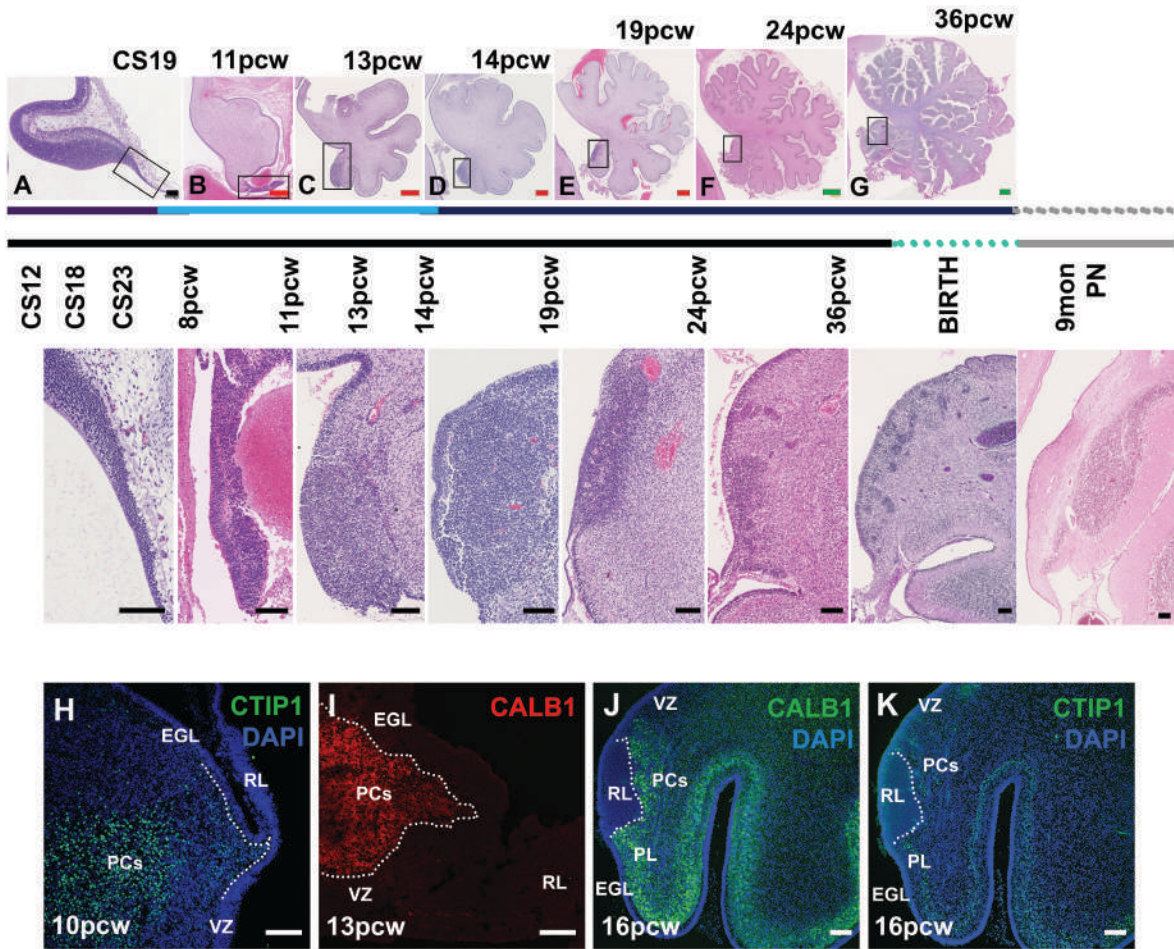
Figure 3

Fig. 3: Spatio-temporal expansion of the human cerebellar rhombic lip. The human cerebellar RL undergoes morphological transformations during development and provides granule cell precursors to the external granule layer. The human RL structurally resembles the mouse RL at CS19 (A). Between 8 and 12 pcw, it is elongated into a 'tail-like' structure (B, box). After 13 pcw the RL internalizes to form a pool of cells confined to the posterior-most lobule (C-G, box). The RL is not seen after birth (H). Purkinje cells (PCs) born in the ventricular zone (VZ), as indicated by CTIP1 (H, K) and CALB1 [Calbindin] (I, J) expression can be seen migrating around the RL region. Scale bar = 100 µm (A, black; H-K, white,), 500 µm (B-E, red), and 1 mm (F, G, green)
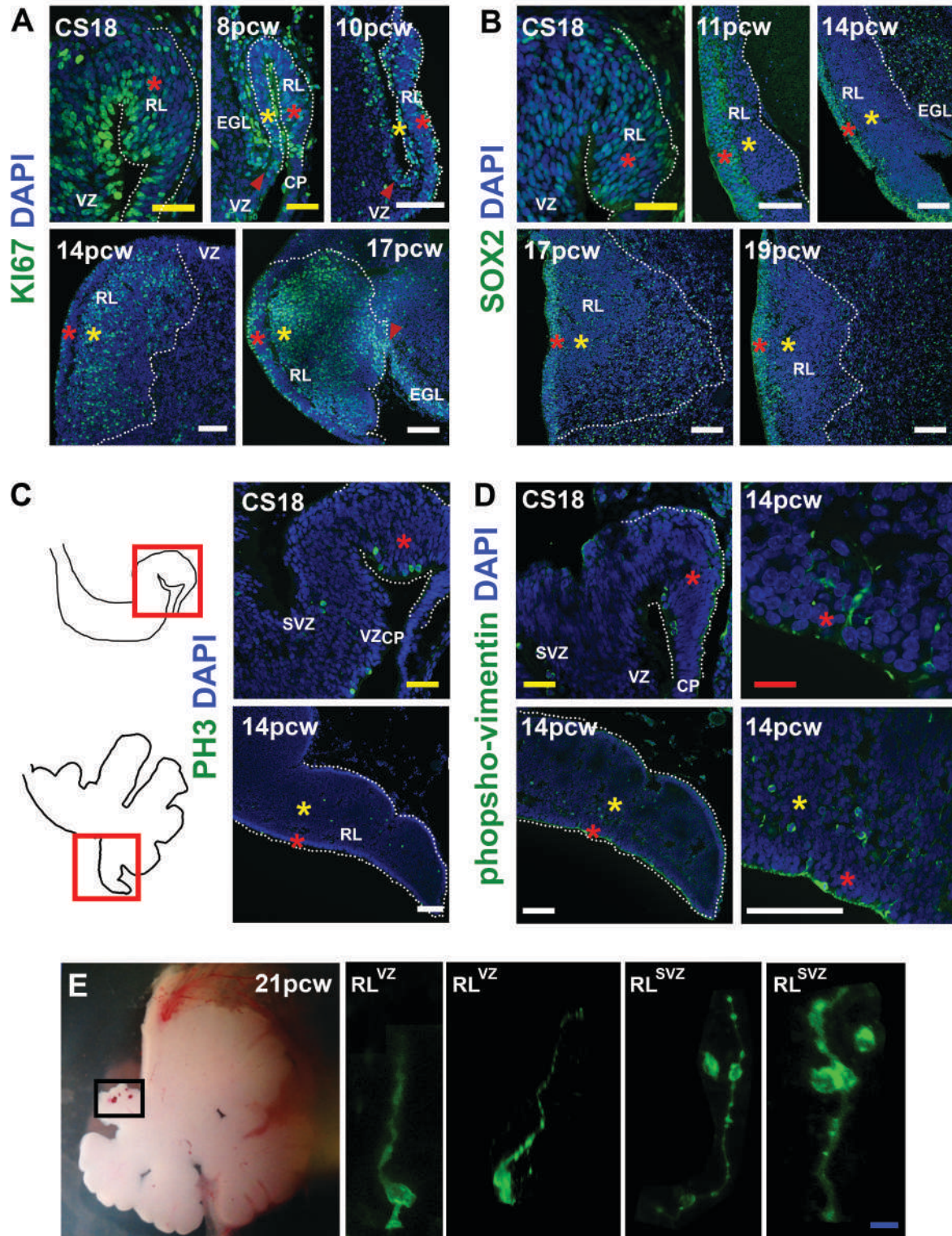
Fig. 4: The human cerebellar rhombic lip is compartmentalized into ventricular and subventricular zones. The human cerebellar RL is highly proliferative as indicated by KI67 expression (A). The RL is expanded into a SOX2-rich ventricular (red asterisk) and SOX2-sparse (yellow asterisk) subventricular zones (B). phosphohistone-H3 (C) and phospho-vimentin

(D) expression indicate the presence of ventricular (red asterisk) and outer radial glia (yellow asterisk) in a state of mitosis. DiI labeling of an organotypic slice of a 21 pcw human cerebellum (E) reveals morphology of ventricular and outer radial glia in the RL. Scale bar = 100 μm (white), 50 μm (yellow), 20 μm (red), and 1 μm (blue).
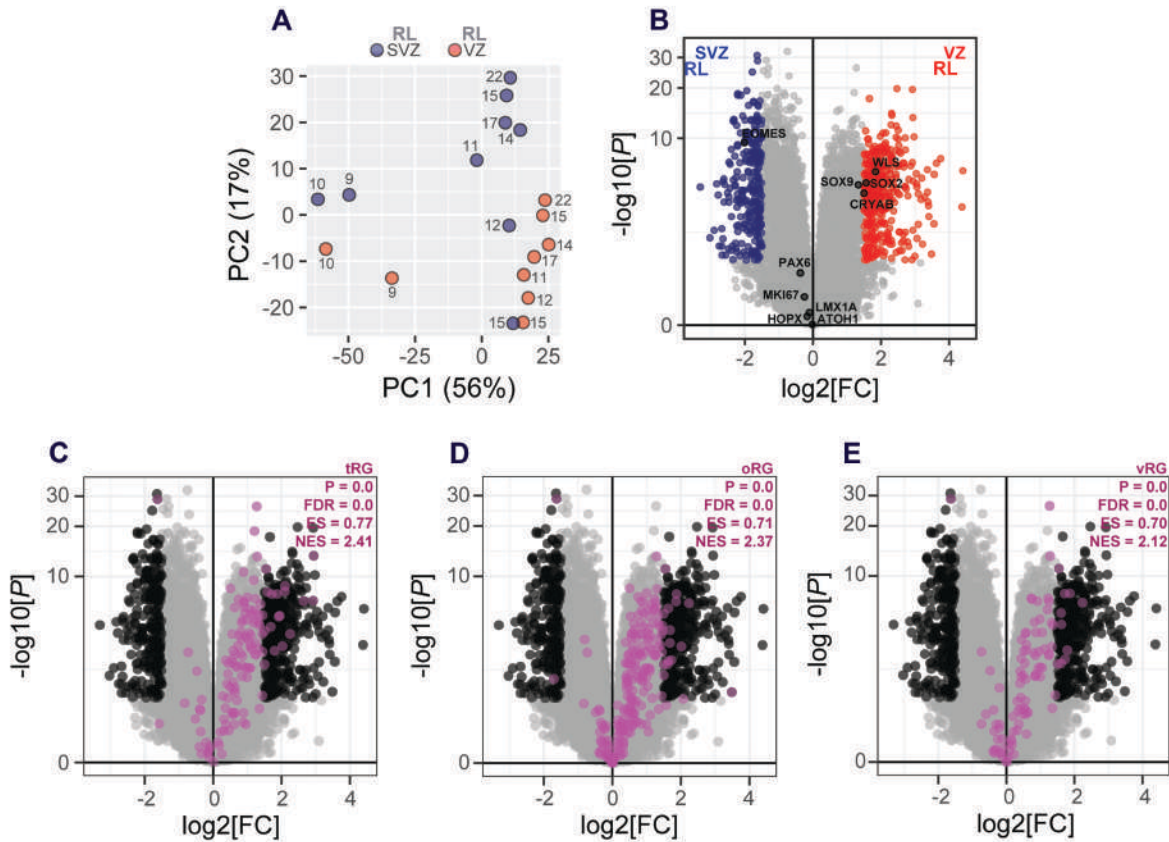
5

Figure 5

Fig. 5: RNA-seq of human cerebellar RL compartments. (A) Principal component (PC) analysis indicated that the largest source of variation among the RNA-seq samples was age accounting for 56% of the variance in the data. Samples microdissected from RL^{SVZ} are blue and RL^{VZ} are red. The numbers beside each circle represent age of the sample in pcw. (B) Volcano plot illustrating differential expression of genes in RL^{VZ} versus RL^{SVZ}. Red and blue dots represent genes expressed significantly higher in RL^{VZ} or RL^{SVZ}, respectively. (C-E) Comparison of the human RL expression profile to human cortical radial glia. Volcano plot illustrating differential expression of genes in RL^{VZ} versus RL^{SVZ}. Black dots represent genes with significant differential expression between RL^{VZ} and RL^{SVZ}. Purple dots represent genes from each gene set. GSEA showed that human cortical radial glia genes are all enriched in the RL^{VZ}.
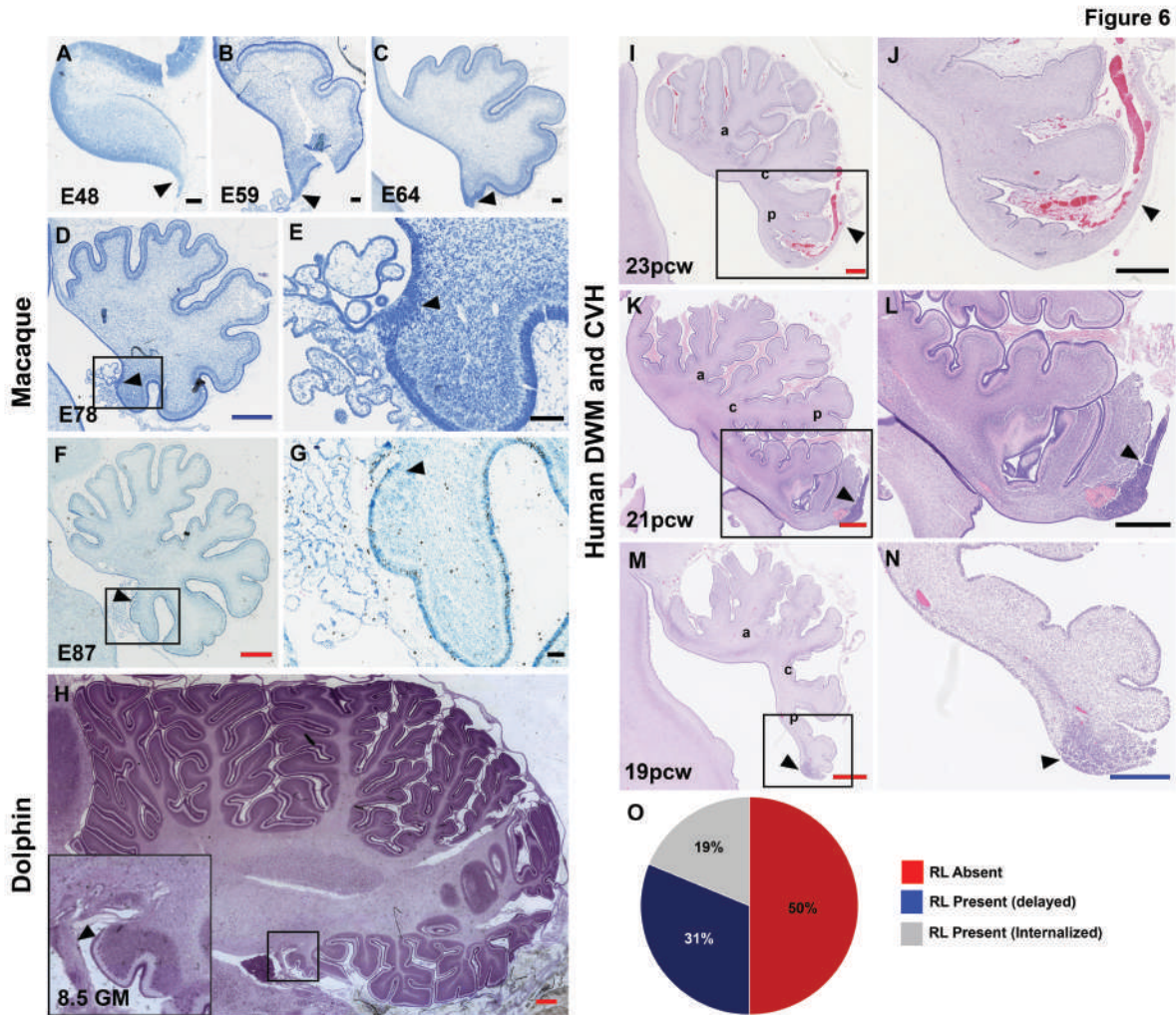
20

Fig. 6: Internalized rhombic lip is a feature specific to human cerebellar development. Cresyl violet-stained sagittal sections of the developing macaque cerebellum at (A) E48, (B) E59, (C) E64, (D, E) E78, (F, G) E87, and (H) H&E-stained sagittal section of the cerebellum from a bottlenose dolphin of age 8.5 gestational months (GM) suggests that the rhombic lip is not a feature of all primates or animals with a prolonged gestation period, but rather a human-specific trait. Analysis of H&E-stained sagittal sections of the human cerebellum from cases diagnosed with DWM and CVH (I-N) indicates RL is absent in 50% of cases while in the remaining cases it was severely diminished (O). The anterior (a), central (c) and posterior lobes (p) are indicated. (O) Pie chart representing the absence of rhombic lip in 50% of tested samples. Scale bar = 100 µm (A-C, E, G, J, L, black), 0.5 mm (D, N, blue) and 1 mm (F, H, I, K, M, red)

Supplemental information

Materials and Methods

Human tissue collection: All human samples (80 normal and 16 DWM/CVH) were obtained in accordance with approved IRB protocols at Seattle Children's Research Institute. All 3-20 postconception week (pcw) tissue samples were collected by the Human Developmental Biology Resource (HDBR) located at University College London, and Newcastle University, United Kingdom, and the Brain Defects Birth Laboratory (BDRL) at the University of Washington, Seattle, WA. Mid- and late-gestation samples were part of an archival collection at the Hôpital Necker-Enfants Malades in Paris, France. Samples were collected with previous patient consent and in strict accordance with institutional and legal ethical guidelines. Embryonic samples were staged using the Carnegie staging system, while samples were staged using foot length. The age of the fetus is listed as pcw, which starts from the point at which fertilization took place. There is an approximate 2-week difference between pcw and gestational weeks. Only tissues with no detectable cerebellar pathology following histopathological analyses were included as controls. All Dandy-Walker malformation (DWM) and cerebellar vermis hypoplasia (CVH) samples used in the study were also part of archival collections obtained from pathologists from Italy, France, Israel and the United States, all of whom are authors on this study. Cerebella were fixed in formalin (pH 7.6) and embedded in paraffin. Sagittal sections of 4-5 µm thickness were cut using a microtome (Leica RM 2135) and placed on Superfrost Plus white slides (VWR international, USA). Slides were stored at room temperature until immunostaining was performed.

Animals: Animal experimentation was carried out in accordance with the guidelines laid down by the Institutional Animal Care and Use Committee (IACUC), of Seattle Children's Research Institute, Seattle, WA, USA. CD1 mice were crossed and the day of plug was taken as embryonic day (E) 0.5. Embryos were dissected out between E12.5 and E16.5. Cerebella were dissected postnatally between P0 and P21. Samples were fixed in 4% paraformaldehyde (PFA) overnight, washed in PBS and sunk in 30% sucrose. Tissue was subsequently embedded in optimum cutting temperature (OCT) compound and midsagittal cryosections of 11 µm were collected. Images of the developing rhesus macaque cerebellum were obtained from the MacBrain resource (https://medicine.yale.edu/neuroscience/macbrain/), an extensive archival collection of macaque brain samples collected by Profs Rakic and Goldman-Rakic at the Department of Neuroscience at Yale University. Cresyl violet-stained sagittal sections of the bottlenose dolphin (*Tursiops truncatus*), part of the Glezer-Morgane collection, were imaged at the Hof laboratory in New York. The full brain was collected in the 1960s by Drs Peter Morgane and Myron Jacobs. The sample available to us was embedded in celloidin and sectioned on a sliding microtome at 35 µm thickness, stained with cresyl violet, and mounted on thick glass.

Histology: Human cerebellar tissue was fixed in 4% PFA and then processed through graded alcohols and changes of xylene and paraffin wax. Processed tissue was then embedded in paraffin wax prior to sectioning. Samples sectioned using the cryostat were treated with 30% sucrose following fixation. Paraffin sections were collected at 4 µm, while cryosections were collected at 12 µm. Cresyl violet and H&E staining were carried out as previously described (Haldipur et al., 2011).

1

Immunohistochemistry: Immunohistochemistry was performed as previously described (Haldipur et al., 2011)**.** Briefly, sections were subjected to antigen retrieval followed by blocking and permeabilization with 5% normal goat serum containing 0.35% triton X. Primary antibodies were incubated overnight at 4ºC. We used primary antibodies against KI67 (DAKO, M7240, mouse, 1:50), SOX2 (Thermofisher, PA1-094, Rabbit, 1:200), β-III Tubulin (Promega, G712A, Mouse, 1:1000), Calbindin (Swant, CD38, rabbit,1:3000), phospho-histone H3 (Cell signalling technologies, 9706S, rabbit, 1:100), CTIP1 (Abcam, ab19489, rabbit, 1:100), Wntless (Seven Hills Bioreagents, WLAB-177, rabbit, 1:100), PAX6 (Biolegend, 901301, rabbit, 1:300), TBR2 (Thermofisher, 14-4875-82, mouse,1:250), vimentin (Abcam, ab92547, rabbit, 1:200), GFAP (DAKO, Z0034, rabbit, 1:1000), CD34 (DAKO, M716501-2, Mouse, 1:100) and phospho-vimentin (MBL, D076-3, mouse, 1:200). Species and subtype-appropriate fluorescent dye-labelled secondary antibodies were used (Alexa Fluor 488 and 594, 1:1000, Molecular probes). Sections were counterstained with DAPI (4',6-diamidino-2-phenylindole) using Vectashield mounting medium with DAPI (Vector laboratories).

DiI labeling: DiI labeling was carried out as described in Saito et al. (Saito et al., 2003). Briefly, 500 μm- to 1 mm-thick sagittal slices of the cerebellum were collected from a 21 pcw cerebellum and incubated in DMEM medium containing fine crystals of DiI (D-282, Molecular Probes, USA) for 10-20 minutes on ice. Tissue was then washed in DMEM containing 10% fetal bovine serum and cultured overnight at 37^0C in 5% CO_2. Slices were then fixed and subsequently imaged using Zeiss LSM 880 confocal microscope.

***In situ* hybridization:** Assays were run using commercially available probes from Advanced Cell Diagnostics. Protocols recommended by the manufacturer were used without modification. The following probes were used in the study *LMX1A* (#540661), *MKI67* (#591771) and *ATOH1* (#417861).

Microscopy: All slides from immunohistochemical assays were imaged using the Zeiss LSM-Meta confocal microscope and ZEN 2009 software (Zeiss). Brightfield microscopy was carried out at 20X magnification using a Nanozoomer Digital Pathology slide scanner (Hamamatsu; Bridgewater, New Jersey). Apart from minor adjustments of contrast and brightness, there was no additional image alteration.

Laser-capture microdissection (LCM): The whole cerebellum was dissected (Data S1) and embedded in OCT, frozen at -80°C, and cryosectioned at 16-μm in the sagittal plane through the cerebellar vermis onto PEN Membrane Glass Slides (Applied Biosystems, USA). Total RNA was isolated from one whole section using the Qiagen RNeasy Micro Kit and RNA quality was assessed using the Agilent Bioanalyzer 6000 Pico Kit before proceeding with LCM. Mean RNA integrity number (RIN) was 7.63±0.79 (s.d.) among the 9 samples. LCM was performed using the Leica DM LMD-6000 Laser Microdissection system to capture RL^{VZ} and RL^{SVZ} regions into separate collection tubes. Total RNA was then isolated from LCM-enriched samples pooled across each sample using the Qiagen RNeasy Micro Kit and RNA quality was assessed using the Agilent Bioanalyzer 6000 Pico Kit.

RNA sequencing: Sequencing libraries were prepared using the Illumina TruSeq RNA Access Prep Kit (Illumina, USA) and 25 ng of total RNA per sample (N=18), according to the manufacturer's protocol. RNA libraries were barcoded and sequenced including 6-8 samples per lane on an Illumina HiSeq 2000 by the Northwest Clinical Genomics Laboratory at the University of Washington. Paired-end reads (100 bp) were aligned to the *Human* reference genome (NCBI build 37/hg19) using STAR (Dobin et al., 2013). Genes counts were summarized using HTSeq (Anders et al., 2015). Gene-level differential expression was analyzed using DESeq2 (Love et al., 2014). Genes with log2 fold change 1.5, *P* value < 0.05 and false discovery rate (FDR) < 0.05 were considered to be differentially expressed. Significant results are reported as Benjamini-Hochberg adjusted *P* values (FDR). Gene Ontology (GO) term and pathway enrichment analysis was performed using the STRING database of protein-protein interactions (https://string-db.org/) (Szklarczyk et al., 2019). REVIGO (http://revigo.ibr.hr) was used to summarize GO results into non-redundant terms (Supek et al., 2011). Gene set enrichment analysis (GSEA) was performed based on the cerebral cortex radial glia gene sets defined in Nowakowski et al (Nowakowski et al., 2017). **(Data S1-S5)**.

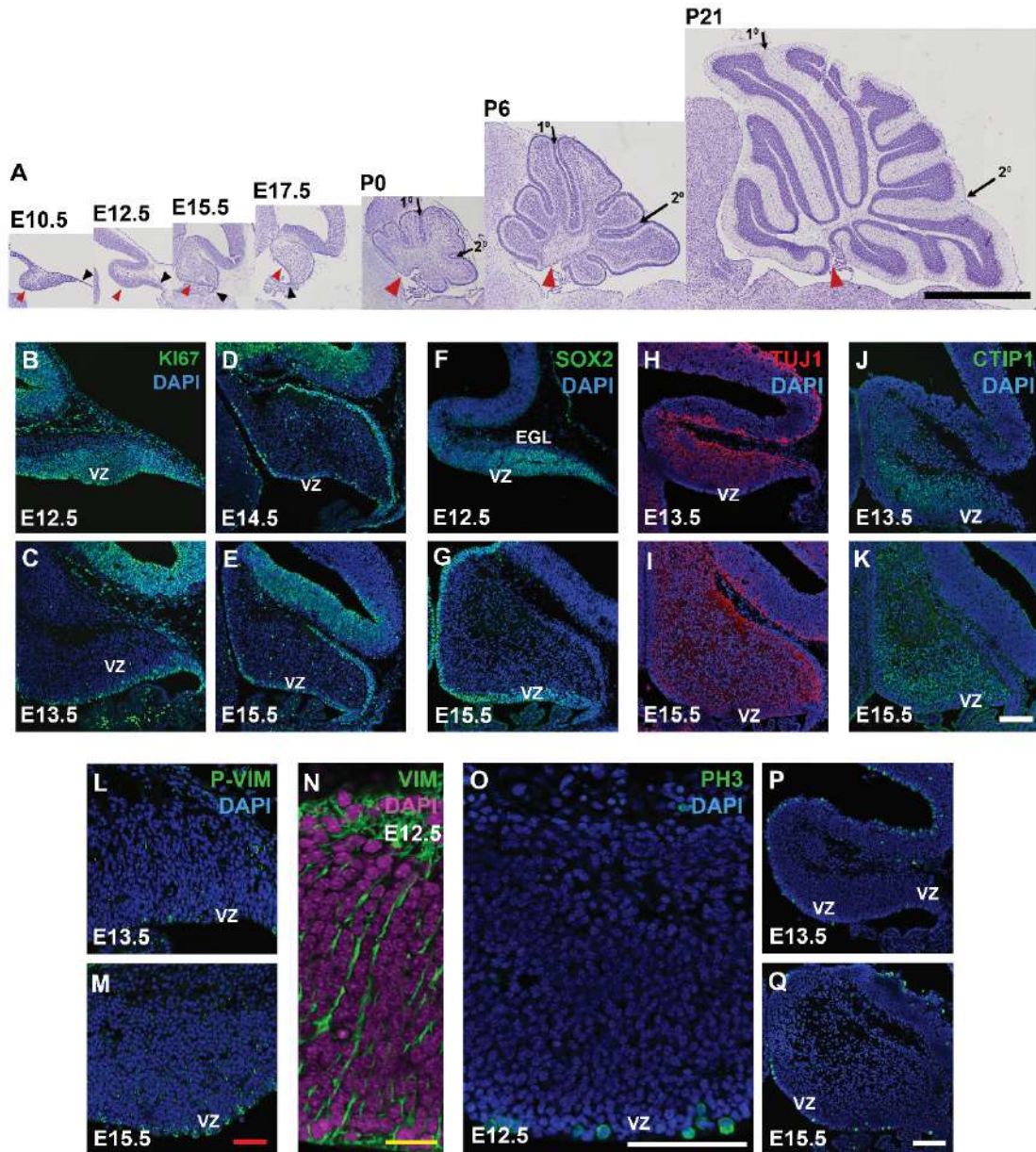**Supplementary Figures: Fig. S1.**

Fig. S1: An outline of mouse cerebellar development. Cresyl violet-stained midsagittal sections through the mouse embryonic (E10.5-E17.5) and postnatal (P0-P21) cerebellum indicates the transient presence of the ventricular zone (red arrowhead) and rhombic lip (black arrow head). Primary and secondary fissures are noted (arrows). KI67 (B-E) and SOX2 (F-G) staining indicate the cerebellar VZ shrinks in thickness after E12.5, with a 2-4 cell layer thick structure lining the ventricle. Neuronal differentiation takes place directly above the VZ as indicated by TUJ1 (H-I) and CTIP1 (J-K) expression. Expression of phospho-vimentin (L,M) – which marks mitotic radial glia, and phospho-histone- H3 (O-Q) which marks all cells in mitosis indicating that mitosis is only confined to the cerebellar VZ thus indicating the lack of a subventricular zone in the mouse cerebellum. Radial glial fibers span the length of the cerebellar anlage as evinced by vimentin staining (N). Scale bar = 100 μm (A-K, O-Q, black/white), 50 μm (L-M, red) and 20 μm (N, yellow).
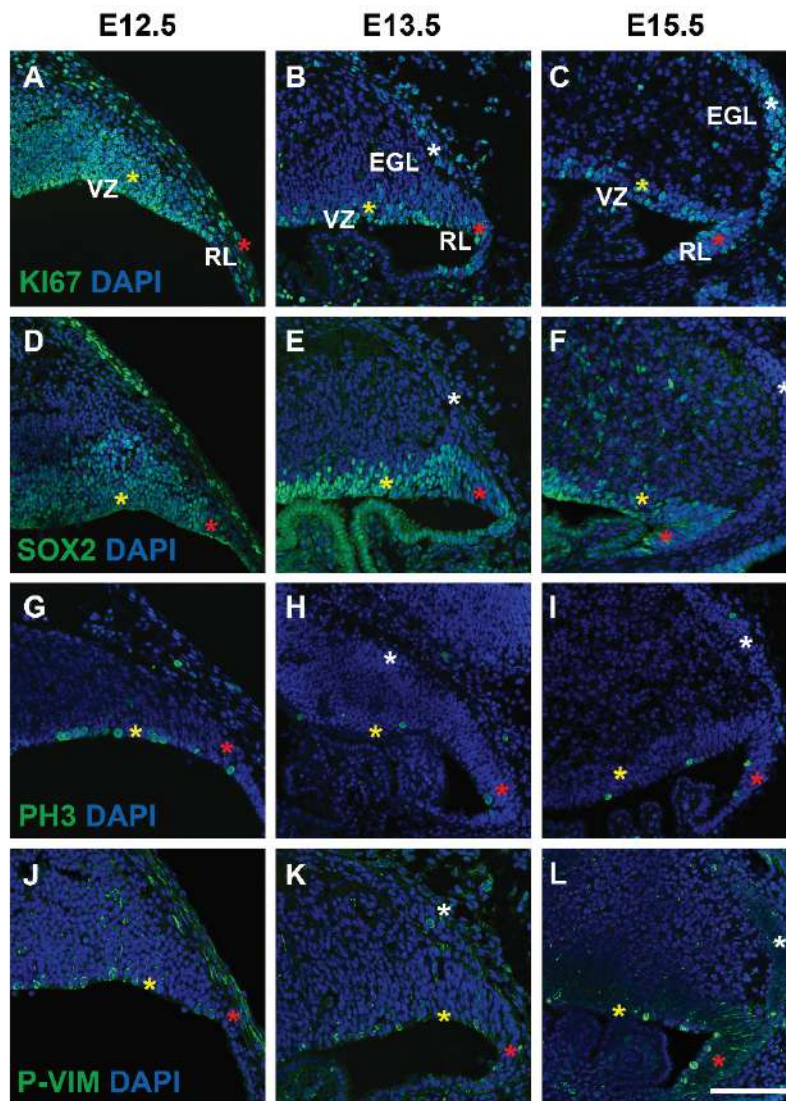
Fig. S2: Rhombic lip development in the mouse. Expression of KI67 (A-C) and SOX2 (B-F) throughout the mouse cerebellar RL (red asterisk) shows that the RL in mouse consists of a layer of proliferative cells and lacks structural compartmentalization. Expression of phospho-histone H3 (G-H, red asterisk) and phospho-vimentin (J-L, red asterisk) shows mitosis is only confined to the layer of RL cells lining the ventricle. Mitosis is also exhibited once cells exit the RL and enter the EGL (G-L white asterisk). Scale bar = 100 μm
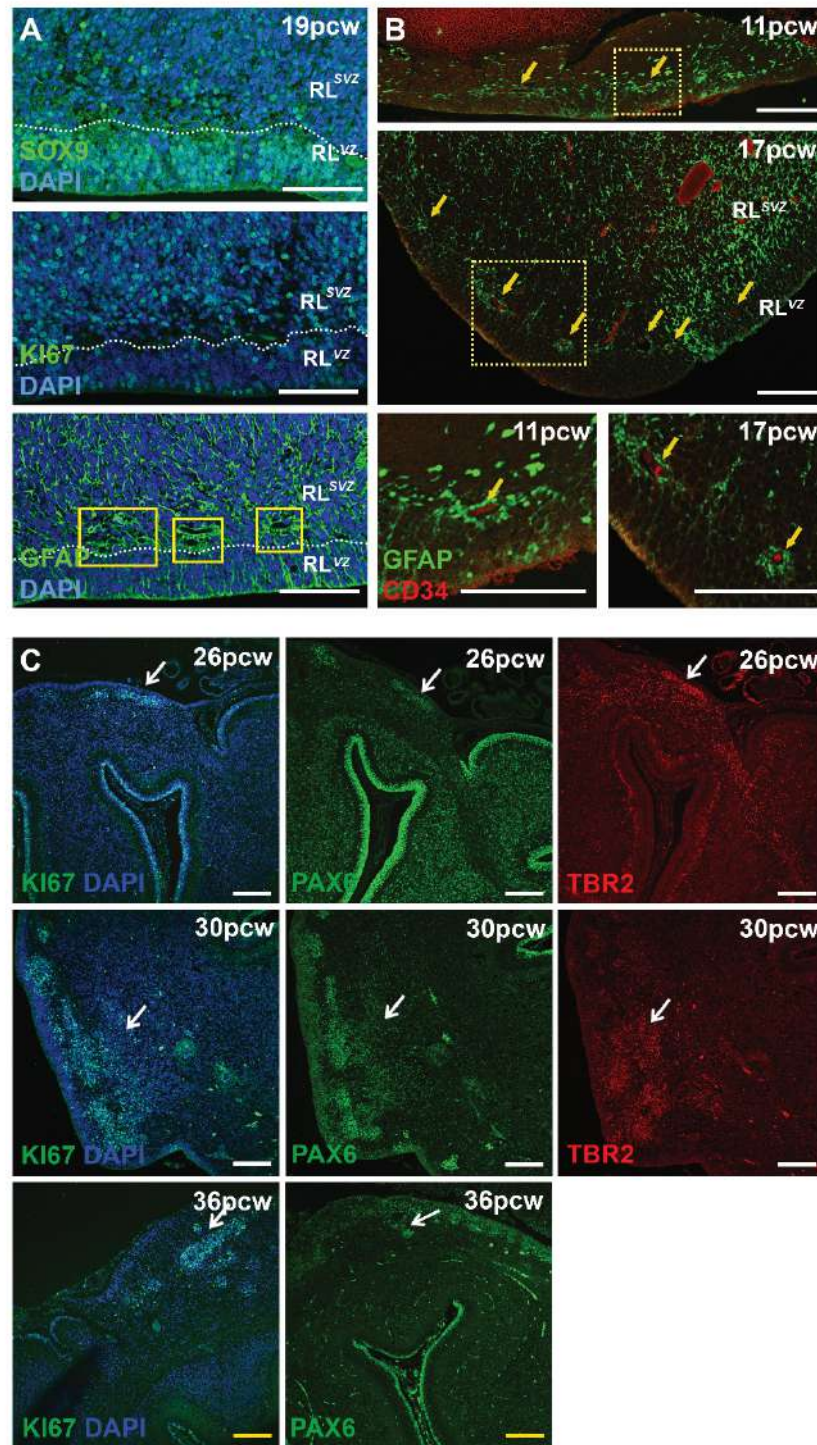
Fig. S3.

Fig. S3: The human rhombic lip is a highly vascularized region and it persists until birth. The human cerebellar rhombic lip is structurally compartmentalized into a ventricular (RL^{VZ}) and subventricular zones (RL^{SVZ}) (A). The two compartments are separated by a lining of blood vessels and glia as indicated by GFAP (A, B) and CD34 expression (B). Although the structure of the rhombic lip changes over time, it persists until birth as indicated by KI67, PAX6 and TBR2 staining (C). Scale bar = 100 μm (white) and 200 μm (yellow).
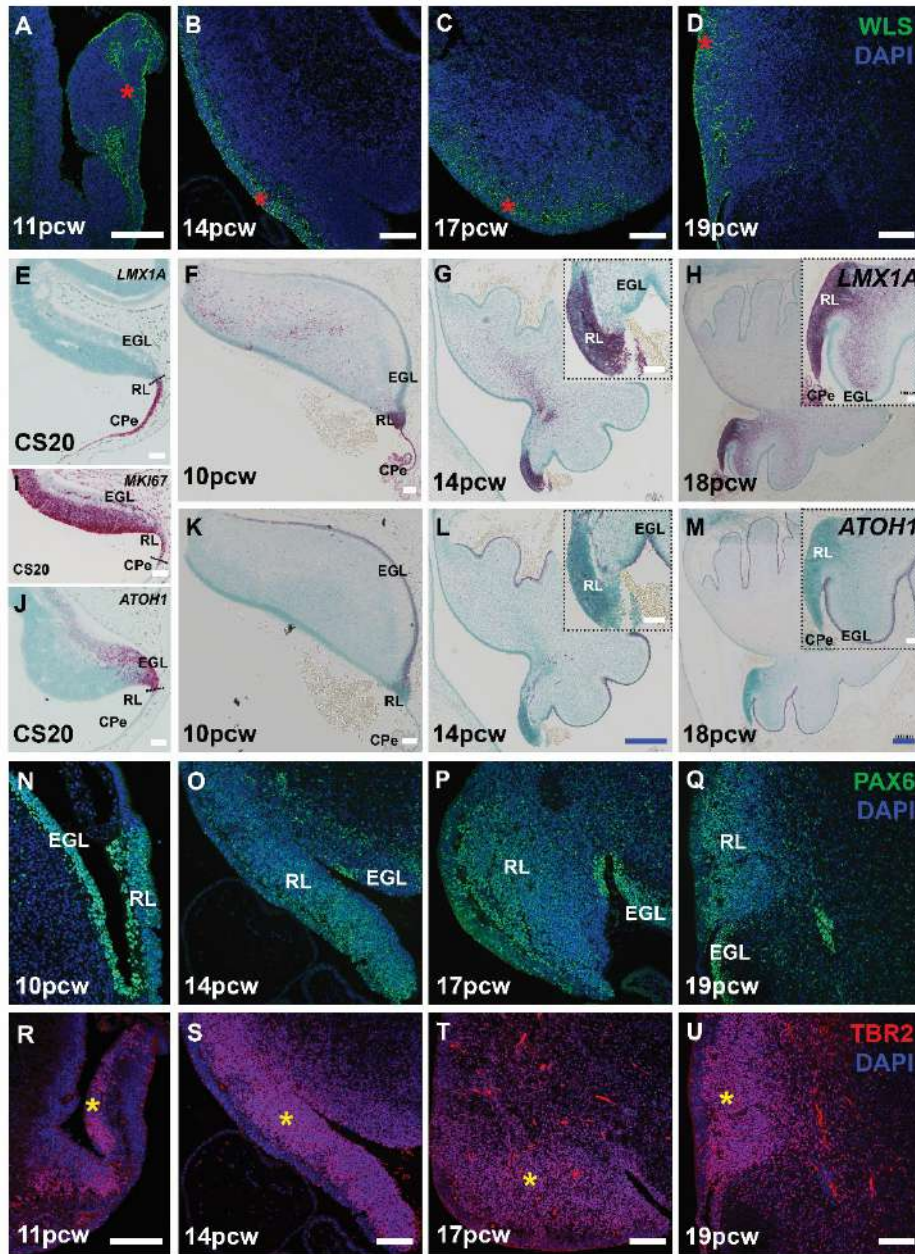
Fig. S4: Expression of selected genes in the human cerebellar rhombic lip. Wntless (A-D) expression in the in the human RL. *LMX1A* (E-H) and *ATOH1* (J-M) expression as detected by *in situ* hybridization can be used to define the boundary between the RL and EGL, with LMX1A marking all RL and Unipolar brush cells that migrate into the cerebellar anlage core, and ATOH1 specifically marking cells exiting the RL and specifically the granule cell precursors of the EGL. *MKI67* expression defines the boundary of the rhombic lip and choroid plexus epithelium (I, black line, CPe). PAX6 (N-Q) and TBR2 (R-U) which are highly expressed in the mouse RL are also expressed in the human RL. The RL shows high expression of PAX6 in both the RL^{VZ} and RL^{SVZ} (N-Q). PAX6 expression persists in all RL derivatives including the GCPs of the EGL (O-Q, EGL). WLS and TBR2 on the other hand are differentially expressed in the RL^{VZ} (A-D, red asterisk) and RL^{SVZ} (R-U, yellow asterisk) respectively. Scale bar = 100 μm (A-F; I-K; N-U, white), 500 μm (G, H, L and M, blue).
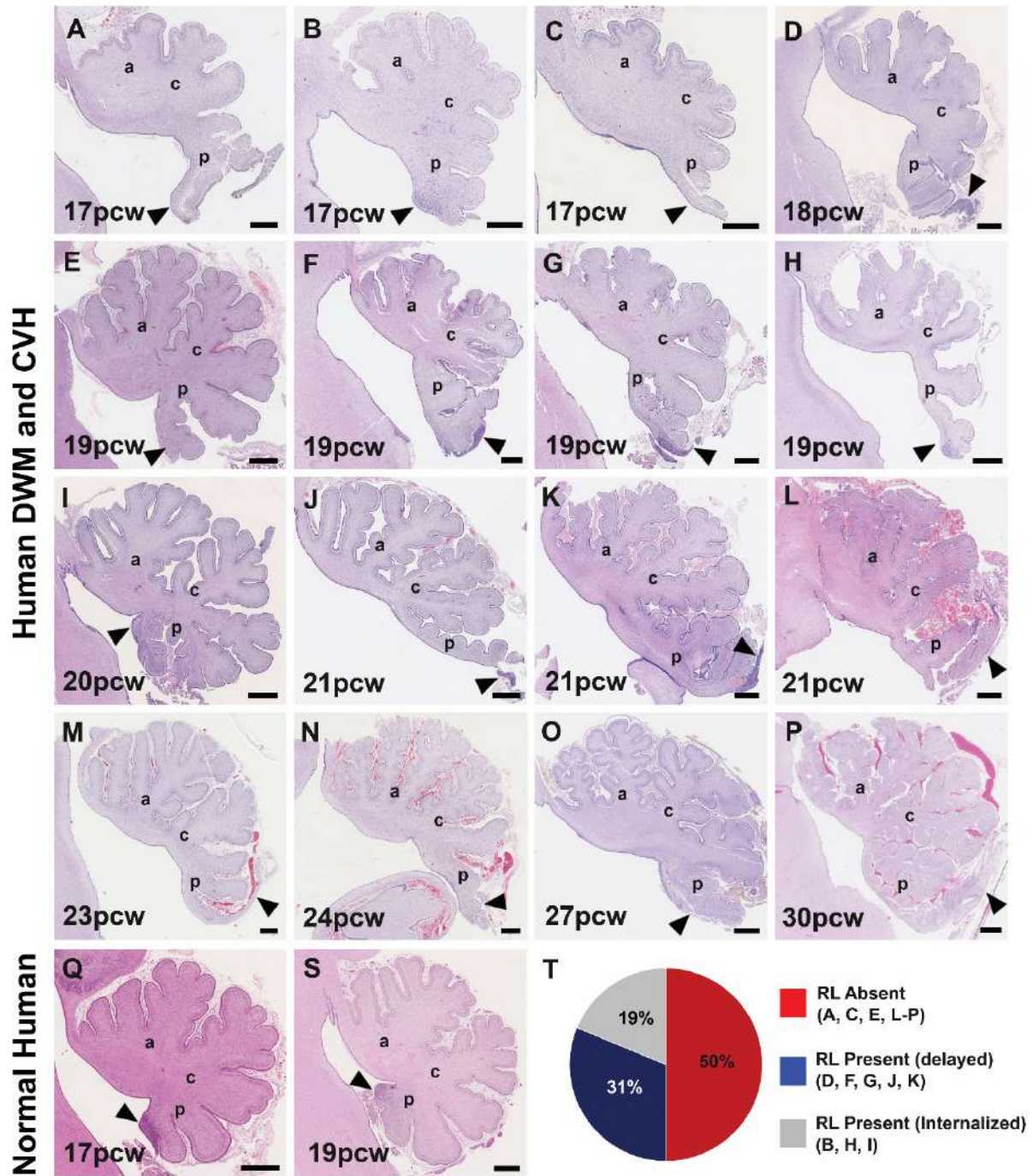
Fig. S5.

Fig. S5: Disruptions in rhombic lip development is associated with cerebellar hypoplasia. (A-P) Analysis of H&E-stained sagittal sections of the human cerebellum from 16 cases diagnosed with DWM (A-D, F-H, J-P) and CVH (E, I) indicates the RL is absent in 50% of cases while in the remaining cases it was severely diminished (T). (Q, S) H&E-stained sections of the normal cerebellum. (Y) Graph representing the absence of rhombic lip in 50% of tested samples. The anterior (a), central (c) and posterior lobes (p) are indicated. Scale bar = 1 mm

Table S1: List of samples used in the study

Species	Age	Number of samples	Feature
Human	CS12	1	Normal
Human	CS14	2	Normal
Human	CS16	3	Normal
Human	CS17	1	Normal
Human	CS18	3	Normal
Human	CS19	3	Normal
Human	CS20	3	Normal
Human	CS21	2	Normal
Human	CS22	1	Normal
Human	CS23	3	Normal
Human	8 pcw	1	Normal
Human	9 pcw	2	Normal
Human	10 pcw	3	Normal
Human	11 pcw	4	Normal
Human	12 pcw	2	Normal
Human	13 pcw	4	Normal
Human	14 pcw	6	Normal
Human	15 pcw	2	Normal
Human	16 pcw	2	Normal
Human	17 pcw	6	Normal
Human	18 pcw	4	Normal
Human	19 pcw	4	Normal
Human	20-24 pcw	8	Normal
Human	25-32 pcw	6	Normal
Human	33-40 pcw	5	Normal
Human	17 pcw	3	Dandy Walker malformation
Human	18 pcw	1	Dandy Walker malformation
Human	19 pcw	3	Dandy Walker malformation
Human	19 pcw	1	Cerebellar vermis hypoplasia
Human	20 pcw	1	Cerebellar vermis hypoplasia
Human	21 pcw	3	Dandy Walker malformation
Human	23 pcw	1	Dandy Walker malformation
Human	24 pcw	1	Dandy Walker malformation
Human	27 pcw	1	Dandy Walker malformation
Human	30 pcw	1	Dandy Walker malformation
Rhesus macaque	Embryonic day 48	1	Normal
Rhesus macaque	Embryonic day 59	1	Normal
Rhesus macaque	Embryonic day 64	1	Normal
Rhesus macaque	Embryonic day 78	1	Normal
Rhesus macaque	Embryonic day 87	1	Normal

Bottlenose dolphin	8.5 gestational months	1	Normal

Data S1-S5. (separate file)

Data S1: List of samples used for RNA seq analysis

Data S2: RL transcriptome differential gene expression analysis

Data S3: Biological process and pathway enrichment among RL^{VZ} genes

Data S4: Biological process and pathway enrichment among RL^{SVZ} genes

Data S5: Cerebral cortex radial glia gene lists from Nowakowski et al. (Nowakowski et al., 2017) used in GSEA

References

Anders, S., Pyl, P. T. and Huber, W. (2015) 'HTSeq--a Python framework to work with high-throughput sequencing data', *Bioinformatics* 31(2): 166-9.

Dobin, A., Davis, C. A., Schlesinger, F., Drenkow, J., Zaleski, C., Jha, S., Batut, P., Chaisson, M. and Gingeras, T. R. (2013) 'STAR: ultrafast universal RNA-seq aligner', *Bioinformatics* 29(1): 15-21.

Haldipur, P., Bharti, U., Alberti, C., Sarkar, C., Gulati, G., Iyengar, S., Gressens, P. and Mani, S. (2011) 'Preterm delivery disrupts the developmental program of the cerebellum', *PloS one* 6(8): e23449.

Love, M. I., Huber, W. and Anders, S. (2014) 'Moderated estimation of fold change and dispersion for RNA-seq data with DESeq2', *Genome biology* 15(12): 550.

Nowakowski, T. J., Bhaduri, A., Pollen, A. A., Alvarado, B., Mostajo-Radji, M. A., Di Lullo, E., Haeussler, M., Sandoval-Espinosa, C., Liu, S. J., Velmeshev, D. et al. (2017) 'Spatiotemporal gene expression trajectories reveal developmental hierarchies of the human cortex', *Science* 358(6368): 1318-1323.

Saito, K., Kawaguchi, A., Kashiwagi, S., Yasugi, S., Ogawa, M. and Miyata, T. (2003) 'Morphological asymmetry in dividing retinal progenitor cells', *Development, growth & differentiation* 45(3): 219-29.

Supek, F., Bosnjak, M., Skunca, N. and Smuc, T. (2011) 'REVIGO summarizes and visualizes long lists of gene ontology terms', *PloS one* 6(7): e21800.

Szklarczyk, D., Gable, A. L., Lyon, D., Junge, A., Wyder, S., Huerta-Cepas, J., Simonovic, M., Doncheva, N. T., Morris, J. H., Bork, P. et al. (2019) 'STRING v11: protein-protein association networks with increased coverage, supporting functional discovery in genome-wide experimental datasets', *Nucleic acids research* 47(D1): D607-D613.